Published in final edited form as:
J Bone Miner Res. 2014 May ; 29(5): 1118–1130. doi:10.1002/jbmr.2113.

Interdependence of Muscle Atrophy and Bone Loss Induced by Mechanical Unloading

Shane A. Lloyd, Ph.D.[1], **Charles H. Lang, Ph.D.**[2], **Yue Zhang, Ph.D.**[1], **Emmanuel M. Paul, B.S.**[1], **Lacee J. Laufenberg, M.D.**[2], **Gregory S. Lewis, Ph.D.**[1], and **Henry J. Donahue, Ph.D.**[1,2]

[1]Division of Musculoskeletal Sciences, Department of Orthopaedics and Rehabilitation, Penn State College of Medicine, 500 University Drive, Hershey, PA 17033

[2]Departments of Cellular and Molecular Physiology and Surgery, Penn State College of Medicine, 500 University Drive, Hershey, PA 17033

Abstract

Mechanical unloading induces muscle atrophy and bone loss; however, the time course and interdependence of these effects is not well defined. We subjected 4-month-old C57BL/6J mice to hindlimb suspension (HLS) for three weeks, sacrificing 12-16 mice on day (D) 0, 7, 14, and 21. Lean mass was 7-9% lower for HLS vs. control from D7-21. Absolute mass of the gastrocnemius (gastroc) decreased 8% by D7, and was maximally decreased 16% by D14 of HLS. mRNA levels of Atrogin-1 in the gastroc and quad were increased 99% and 122%, respectively, at D7 of HLS. Similar increases in MuRF1 mRNA levels occurred at D7. Both atrogenes returned to baseline by D14. Protein synthesis in gastroc and quad was reduced 30% from D7-14 of HLS, returning to baseline by D21. HLS decreased phosphorylation of SK61, a substrate of mammalian target of rapamycin (mTOR), on D7-21, while 4E-BP1 was not lower until D21. Cortical thickness of the femur and tibia did not decrease until D14 of HLS. Cortical bone of controls did not change over time. HLS mice had lower distal femur bone volume fraction (−22%) by D14; however, the effects of HLS were eliminated by D21 due to the decline of trabecular bone mass of controls. Femur strength was decreased approximately 13% by D14 of HLS, with no change in tibia mechanical properties at any time point. This investigation reveals that muscle atrophy precedes bone loss during unloading and may contribute to subsequent skeletal deficits. Countermeasures that preserve muscle may reduce bone loss induced by mechanical unloading or prolonged disuse. Trabecular bone loss with age, similar to that which occurs in mature astronauts, is superimposed on unloading. Preservation of muscle mass, cortical structure, and bone strength during the experiment suggests muscle may have a greater effect on cortical than trabecular bone.

Keywords

muscle atrophy; bone loss; unloading; microgravity; hindlimb suspension

CORRESPONDING AUTHOR: Henry J. Donahue, Ph.D. Division of Musculoskeletal Sciences Department of Orthopaedics and Rehabilitation Penn State College of Medicine 500 University Drive, Hershey, PA 17033 Telephone: 717-531-4819 Fax: 717-531-7583 hdonahue@psu.edu.

Disclosures: The authors have no financial interests or conflicts of interest to disclose.

INTRODUCTION

Prolonged bed rest as a result of neurological injury or trauma results in significant deleterious effects on bone mass and strength (1,2). Similarly, “weightlessness” encountered during spaceflight leads to bone loss at a rate of 0.5-1.5% per month (3). Furthermore, Lang *et al.* found that a year after 4 to 6-month stays on the International Space Station, astronaut femoral bone mineral density had only partially recovered (4). Unloading-induced bone loss results from the uncoupling of bone turnover: bone formation decreases, while bone resorption increases (5).

In addition to bone loss, there is the well-documented development of muscle atrophy during spaceflight. Astronauts on a 17-day shuttle mission experienced a 10% decrease in strength of knee extensor muscles and an 8% decrease in cross-sectional area (6), while astronauts on an 8-day mission saw muscle volume decline 4-8% (7). Other studies have examined sarcopenia following spaceflight (8,9), extended best rest (10), or spinal cord injury (11). Muscle atrophy combined with bone loss may increase the risk for fracture during a spaceflight mission or following return to Earth (12).

Numerous pharmacological, exercise, and nutritional strategies have been evaluated to mitigate the musculoskeletal effects of mechanical unloading with variable success (13). It is clear that a better understanding of the fundamental structural, functional, and molecular changes occurring to muscle and bone during spaceflight or clinical disuse, along with a time course of these effects, is necessary to better define the problem and aid in the development of more effective countermeasures. Muscle and bone are intimately involved organs, from their anatomical, biochemical, and functional relationship, to their development from common mesenchymal origins (14). Effective therapeutic interventions to prevent muscle atrophy and bone loss will leverage this interdependence to maximize efficacy.

Due to the high cost, there is a limited data set regarding the physiological response to spaceflight. A need for ground-based models of microgravity led to the development of the hindlimb suspension (HLS) model by Morey-Holton *et al.* (15). In this model, a device is attached to the animal's tail, such that hindlimb weight bearing is prevented. However, unlike other models of unloading, such as neurectomy, casting, or botulinum toxin (botox) paralysis, the hindlimbs are not immobilized. Thus, much like spaceflight, passive muscle forces are allowed to continue. Animals also experience a cephalic fluid shift during HLS. This feature is relevant given that reduced skeletal perfusion may contribute to musculoskeletal changes during spaceflight (16). Most importantly, HLS induces significant and reproducible muscle atrophy and bone loss (17,18). HLS also has important limitations when compared to other disuse models such as botox. For example, HLS is more technically difficult, requiring specialized enclosures and apparatus, and induces relatively modest bone loss (19). The HLS technique also requires close observation of animal health by experienced individuals to avoid excessive weight loss or issues with reduced tail perfusion and necrosis owing to the suspension apparatus. Despite these limitations, HLS has evolved as the standard for simulation of microgravity in rodents.

Ground-based unloading studies offer numerous advantages when compared with spaceflight studies, including lower cost, reproducibility, extended duration, easy tissue collection, and the ability to make longitudinal measurements (15). Despite its proven utility, there has been no detailed, integrated assessment of the temporal effects of HLS on both muscle and bone in mice. This is important considering the relationship between muscle and bone metabolism (20). For example, muscle exerts force on bone during contraction (21), while muscle-secreted factors may also influence bone cell activity (22).

In the present study we have undertaken a comprehensive investigation utilizing the HLS model to develop a better understanding of the time course and potential mechanisms underlying unloading-induced muscle and bone loss. We found that sarcopenia precedes osteopenia during HLS and occurs as a result of increased protein degradation and decreased protein synthesis. In addition, trabecular bone loss that occurs as a result of aging is superimposed on the effects of unloading. This is in contrast to cortical bone and muscle, which did not decline over the experimental period in normally loaded control mice. These findings have refined the HLS model and provide novel insight into the integrated musculoskeletal effects of unloading.

METHODS

Animal Procedures

We utilized male C57BL/6J mice (Jackson Labs; Bar Harbor, ME). Mice were 112±3 days old at day 0. Mice of this age were selected due to their successful use in previous ground-based (23) and spaceflight (24) studies. Mice were fed standard 2018 Teklad Global 18% Protein Rodent Diet (Harlan Laboratories, Inc.; Indianapolis, IN) *ad libitum*, maintained at 25°C, and kept on a 12 hour light/dark cycle. Mice were housed in standard enclosures (2 mice/cage) until one-week prior to experimentation, when the pairs were moved into the HLS enclosures to acclimatize while ambulating normally. Mice were weighed and then assigned to groups (Table 1) to obtain an approximately equal average body weight per group. At day 0, mice assigned to HLS were unloaded. A group of baseline mice was sacrificed at day 0.

Hindlimb Suspension

We used a modified version of the HLS model first described by Morey-Holton *et al.* (15) and described in detail previously (18). Our HLS enclosures consisted of a modified rat cage with standard bedding placed below a wire mesh insert. Two metal crossbars were located at either end of the cage, along with water bottles. Under isoflurane anesthesia (2%), two strips of bandage tape were braided around the tail, with loose ends fixed to a swivel hook attached to a string. The string was wound around the cross bar at the top of the cage. The crossbar could be rotated, raising or lowering the hindquarters of the animal to achieve a 30° elevation. This angle of suspension has been previously demonstrated to keep the forelimbs normally-loaded, while minimizing tail tension and animal stress (25). Two mice were suspended per cage in this manner, although their placement at opposite ends prevented physical contact. Control mice were housed in this same cage environment, albeit without attachment of the HLS apparatus. Animals were inspected daily by laboratory and veterinary

staff and their general level of activity, responsiveness, and appearance was assessed. Of particular concern was the prevention of urethral crusting and potential infections in male mice during the first few days of HLS. The urethra was inspected twice daily and cleaned with sterile gauze and warm 0.9% sterile saline as necessary. Animal procedures adhered to NIH guidelines for the use of experimental animals and were approved by the Penn State Institutional Animal Care and Use Committee (Protocol #2012-033).

Body Composition

Lean, fat, and fluid mass of all mice were measured on day 0, 7, 14, and 21 using ^{1}H-NMR (Bruker Minispec, LF90; Woodlands, TX) as described previously (18).

In Vivo Protein Synthesis

Protein synthesis was determined for the gastrocnemius, quadriceps, and heart using the flooding-dose technique (25). Briefly, mice were injected with an intraperitoneal dose of [^{3}H]-L-phenylalanine (Phe; 150 mM, 30 μCi/mL; 1 mL/100 g BW) and blood and tissues collected 15 min thereafter. Approximately 1-2 min prior to collection of blood, mice were anesthetized with isoflurane (2−3% in oxygen + 1.5% maintenance) and blood collected by percutaneous puncture of the abdominal aorta. Next, gastrocnemius, quadriceps, and heart were excised and frozen using liquid-nitrogen cooled clamps. A portion of each frozen powdered tissue was homogenized in ice-cold 3.6% (w/v) perchloric acid to estimate the rate of incorporation of radioactive Phe into protein. The specific radioactivity of plasma Phe was measured by high-pressure liquid chromatography (HPLC) analysis of supernatant from trichloroacetic acid extracts of plasma, exactly as described (25). The rate of protein synthesis (nmoles Phe incorporated/h/mg protein) was calculated by dividing the amount of radioactivity incorporated into protein by the plasma Phe specific radioactivity. The underlying assumptions for this method and the detailed methodology have been previously reported (26).

RNA Extraction and Real-Time Quantitative PCR

Total RNA was extracted using Trireagent (Molecular Research Center, Inc.; Cincinnati, OH) and an RNeasy mini kit (Qiagen; Valencia, CA). Muscle was homogenized in tri-reagent followed by chloroform extraction. An equal volume of 70% ethanol was then added to the aqueous phase. A Qiagen mini kit protocol was followed from this point, including on-column DNase I treatment. Total RNA (1 μg) was reversed transcribed and RT-qPCR was performed using 25 ng of cDNA for the genes encoding atrogin-1 and muscle RING-finger 1 (MuRF1) as described previously (27). The comparative quantitation method $2^{-\Delta\Delta Ct}$ was used in presenting gene expression in reference to controls (28).

Western Blot Analysis

Muscle was homogenized in ice-cold buffer. Protein concentration was quantified and equal amounts of protein were subjected to SDS-PAGE. Western analysis was performed for phosphorylated 4E-BP1 (Ser65, Bethyl Laboratories; Montgomery, TX) and phosphorylated S6K1 (Thr 389), and total protein of interest or tubulin (Cell Signaling Technology; Boston, MA) used as a loading control. Blots were developed with enhanced chemiluminescence

reagents (Supersignal Pico, Pierce Chemical; Rockford, IL). Dried blots were exposed to x-ray film to achieve a signal within the linear range, scanned, and quantified using Scion Image 3b software (Scion Corp; Frederick, MD). Samples from Control and Suspended mice from the same time point (i.e., day 7, 14, or 21) were run on same gel.

MicroComputed Tomography

Right tibias and femurs were scanned using a Scanco vivaCT 40 (Scanco Medical AG; Brüttsellen, Switzerland). Trabecular bone was assessed in 72 slices of distal femur (immediately proximal to the epiphyseal plate) and proximal tibia (immediately distal to the epiphyseal plate). Cortical bone was assessed in 22 slices of the femur midshaft and tibia (5 mm proximal to the tibia-fibula junction). Settings were: 55 KVp, 145 μA, 200 ms integration time. Images were reconstructed as a matrix of 2048×2048×76 isotropic voxels measuring 10.5 μm. Images were Gaussian filtered (sigma = 1.5, support =2) and a threshold (27.5% of full scale) was used to remove soft tissue. Periosteal and endosteal boundaries of cortical bone were segmented using a semi-automated edge detection algorithm. Trabecular bone was manually segmented. Parameters are reported according to published guidelines (29). Trabecular parameters included bone volume fraction (BV/TV), number (Tb.N), thickness (Tb.Th), separation (Tb.Sp), structure model index (SMI), connectivity density (Conn.D), and tissue mineral density (TMD). Cortical parameters included total area inside the periosteal envelope (Tt.Ar), bone area (Ct.Ar), area fraction (Ct.Ar/Tt.Ar), marrow area (Ma.Ar), thickness (Ct.Th), porosity (Ct.Po), bone mineral density (BMD), and polar moment of inertia (pMOI).

Biomechanical Testing

Bones stored at −80°C after MicroCT scanning were thawed and mechanically tested to failure via three-point bending using a Bose testing apparatus (Bose Corporation, ElectroForce Systems Group; Eden Prairie, MN) (30). Flexural support spans were 8 mm. A loading rate of 1 mm/min was applied in the medial to lateral direction (18). Displacement (d) and force (F) were used to calculate parameters describing whole bone structural properties. Force was converted to bending moment ($M = FL/4$), where L = span length of 8 mm. Displacement was normalized to span length ($d' = 12d/L^2$) (31,32). From a plot of M vs. d', ultimate bending moment, stress, bending rigidity (slope of the linear portion of the curve), total bending energy, ultimate bending energy (area under the curve until the max force), and ultimate normalized displacement (at maximum force) were calculated (31).

Statistical Analysis

Data are shown as mean ± standard error. We used ANOVA with post hoc Student-Neuman-Keuls test when the interaction was significant ($p<0.05$).

RESULTS

Body Mass

Day 0 body mass of Control and Suspended mice was not different (Figure 1A). Body mass of Control mice at each time point did not differ from day 0. Suspended mice had lower

body mass by day 7 (−7%; $p<0.05$) and this reduction was maintained throughout the protocol.

Body Composition: Fluid, Fat, and Lean Mass

Fluid, fat, and lean mass did not differ on day 0 ($p>0.05$ for all; Figure 1B). Fluid mass of Suspended mice decreased by 13% at day 7, with no further change at day 14 (−13%) or day 21 (−12%) ($p<0.05$ for all). Fat mass of Suspended mice decreased 16% at day 7 ($p<0.05$), although Controls lost a similar amount. As Control mice began to recover by day 14, Suspended mice had a fat mass 30% lower than baseline ($p<0.05$) and this remained reduced at day 21 (−25%; $p<0.05$). Lean mass of Suspended mice was 7% lower than baseline by day 7 ($p<0.05$) and remained decreased throughout the protocol.

Muscle Mass and Protein Metabolism

Muscle mass did not change over time for Control mice. By day 7, the absolute mass of the gastrocnemius in Suspended mice was 8% lower than Controls ($p<0.05$) (Figure 2A). By day 14, there was a further decline to −16% ($p<0.05$), with no further decrease at day 21. For the quadriceps, there was no difference between Control and Suspended at day 7 ($p>0.05$), although there was a 14% decrease at day 14 and 21 ($p<0.05$ for both). When normalized to body mass, there was no difference between Control and Suspended gastrocnemius mass at day 7 ($p>0.05$), although it was a significant 5 and 6% lower than Control at day 14 and 21, respectively. The relative quadriceps mass was not significantly different from Control at any of the three sampling times ($p>0.05$).

At day 7, the mRNA content of the gene encoding atrogin-1 was increased in both the gastrocnemius (+199%) and quadriceps (+222%) ($p<0.05$ for both; Figure 2B) of Suspended mice. However, the mRNA level returned to baseline by day 14 and remained unchanged at day 21 for both. The mRNA content of the gene encoding MuRF-1 had a similar temporal response pattern, with a 144% and 188% increase at day 7 for the gastrocnemius and quadriceps ($p<0.05$ for both), returning to baseline levels by day 14 (Figure 2C). There was no change in atrogin-1 or MuRF-1 mRNA levels in normally loaded Control mice at any time point.

The rate of muscle protein synthesis in the gastrocnemius of Suspended mice was 35% lower than Control at day 7 and 28% lower at day 14 ($p<0.05$ for both; Figure 2D). Muscle protein synthesis did not differ between Control and Suspended at day 21. The response was similar in the quadriceps, with an initial decline in muscle protein synthesis of 30% in Suspended ($p<0.05$) and recovery to baseline over the following two weeks. Control animals had no change in muscle protein synthesis over the course of the 21-day protocol.

To determine whether the effect of HLS on skeletal muscle protein synthesis was relatively localized (or specific), we also assessed protein synthesis in cardiac muscle. Myocardial protein synthesis did not differ between Control and Suspended rats at Day 7 (2.00 ± 0.10 vs. 1.82 ± 0.07 nmol/h/mg protein), Day 14 (2.10 ± 0.10 vs. 1.95 ± 0.07 nmol/h/mg protein) or Day 21 (1.99 ± 0.07 vs. 2.2 ± 0.01 nmol/h/mg protein) ($p>0.05$; n=12-16 hearts per group).

The mammalian target of rapamycin (mTOR) is a central regulator of protein synthesis in muscle and its activity can be assessed by determining the phosphorylation state of its downstream substrates, S6K1 and 4E-BP1 (33). HLS decreased Thr-389 phosphorylation of S6K1 in both gastrocnemius and quadriceps muscle by 30−40% at each of the three time points examined ($p<0.05$ for both; Figure 3A,B). In contrast, there were no statistical differences in Ser65-phosphorylation of 4E-BP1 in gastrocnemius and quadriceps muscle at day 7 and 14 of HLS, compared to time-matched control values. However, a significant HLS-induced decrease in phosphorylated 4E-BP1 was detected in both muscles by day 21 ($p<0.05$).

Cortical Bone Microstructure in Control Animals

Most cortical parameters in Control mice did not change with time. Tibia cortical bone mineral density was 1.25% greater than baseline by day 14 ($p<0.05$), with no further change after (Figure 4A). By day 21, tibia polar moment of inertia (pMOI) was 16% lower than day 0 ($p<0.05$). Femur cortical bone responded similarly, with increased mineral density by day 14 and lower pMOI by day 21 (Figure 4B).

Effects of Unloading on Cortical Bone Microstructure

At the tibia, there was no difference for Suspended vs. Control cortical bone at day 7 (Figure 4A). By day 14, Suspended mice had 4% lower cortical area fraction ($p<0.05$). There were non-significant changes in cortical thickness (−4%; $p=0.11$), marrow area (+8%; $p=0.08$), and cortical porosity (−37%; $p=0.09$).

At day 21, tibia cortical thickness of Suspended mice was 7% lower than Control, while cortical area fraction was 5% lower ($p<0.05$ for both). Marrow area was 10% greater than Control at day 21 ($p<0.05$). Other parameters were not different for Control vs. Suspended ($p>0.05$).

Femur cortical response to HLS was similar, although there were no changes detected until day 21 (Figure 4B). At this time, Suspended mice had lower cortical thickness (−7%), lower cortical area fraction (−6%) ($p<0.05$ for both), and a non-significant 8% greater marrow area ($p=0.08$).

Trabecular Bone Microstructure in Control Animals

Trabecular number was the only parameter changed by day 7 at the proximal tibia (−5%; $p<0.05$) (Figure 5A). By day 14, there were also changes in trabecular separation (+13%) and connectivity density (−24%) ($p<0.05$ for both). By day 21, most trabecular parameters had declined below that of baseline, including: trabecular bone volume fraction (−31%), thickness (−13%), number (−11%), separation (+15%), connectivity density (−29%), structure model index (+41%), and tissue mineral density (−23%) ($p<0.05$ for all).

Decline of femur trabecular bone over time was greater, with changes in trabecular separation (+7%), connectivity density (−15%), and structure model index (+28%) by day 7 ($p<0.05$ for all) (Figure 5B). Other parameters, such as trabecular number, bone volume fraction, and tissue mineral density responded similar to the tibia, with the greatest

differences occurring at day 21. Trabecular separation and number were lower at day 7 but did not continue to decrease.

Effects of Unloading on Trabecular Bone Microstructure

Unlike cortical bone, there were significant effects of HLS on trabecular bone at the proximal tibia by day 7 (Figure 5A). Suspended mice had 4% lower trabecular number, 5% higher separation ($p<0.05$ for both) and non-significant changes in bone volume fraction (−12%, $p=0.09$) and tissue mineral density (−19%, $p=0.07$) at day 7.

The difference in trabecular parameters between Suspended and Control were most apparent at day 14. Suspended mice had changes in bone volume fraction (−27%), trabecular thickness (−20%), structure model index (+20%), and tissue mineral density (−21%) ($p<0.05$ for all). Due to the decline of Control trabecular parameters over time, trabecular number and separation, which were significantly different for Suspended mice at day 7, were not different at day 14 ($p>0.05$). By day 21, trabecular parameters in Suspended mice were lower still, although the decline in Control mice resulted in a lower magnitude difference than at day 14. Trabecular separation, connectivity density, and structure model index were not different at day 21.

In trabecular bone at the distal femur, we noted a similar peak difference in microstructural parameters at day 14, with Suspended mice having lower bone volume fraction (−22%), trabecular thickness (−15%), and tissue mineral density (−16%) ($p<0.05$ for all) (Figure 5B); however, by day 21, the decline in ground control trabecular parameters eliminated any differences.

Representative images demonstrate the effect of HLS on cortical and trabecular bone microstructure compared to baseline (Figure 6).

Bone Mechanical Properties

There was no significant change over time in most tibia or femur mechanical properties from controls ($p>0.05$) (Figure 7A,B), with the exception of tibia bending rigidity at day 21, which −21% from baseline ($p<0.05$).

We did not detect any change in mechanical properties of the tibia with unloading. For the femur at day 7, there was a significant difference in stress of femur, which was 8% lower than control ($p<0.05$). It was not until day 14 that most mechanical properties in suspended mice showed any difference from Control. At this time point, femurs had a 13% lower ultimate bending moment, 10% lower stress, and 12% lower bending rigidity ($p<0.05$ for all). The magnitude of the difference for Control vs. Suspended was greater by day 21.

DISCUSSION

In the present study we documented muscle loss beginning as early as one week following the start of HLS. Muscle atrophy occurred concomitant to increased expression of genes associated with protein degradation (i.e., atrogin-1 and MuRF1) and decreased protein synthesis. Changes in muscle preceded those in bone, suggesting that sarcopenia may

contribute to subsequent osteopenia during unloading. Age-related bone loss of normally loaded control mice tended to mask trabecular bone loss during unloading. Conversely, muscle mass, cortical bone structure, and bone strength in control mice did not decline over the experimental period, suggesting the intriguing possibility that muscle may have a greater influence on cortical than trabecular bone. Interestingly, a lack of change in tibia mechanical properties suggests this bone is less sensitive to reductions in strength during HLS.

By day 7 of HLS, we detected a significant decrease in lean body mass. Absolute mass of the gastrocnemius was lower than control at day 7, with suspended mice having the largest reduction in muscle mass at day 14. The quadriceps appeared to be less sensistive to unloading-induced atrophy, with no change in absolute mass until day 14 and no significant change in relative mass at any time point. This is consistent with findings in spaceflight, where loss of muscle volume from the gastrocnemius and soleus of astronauts was found to be twice that of the quadriceps (34). The response of the gastrocnemius was similar to a study by Hanson *et al*., which found 18% lower gastroc mass by day 14 of HLS (35). Ellman *et al*. documented a 15% decline in gastrocnemius mass by day 21 of HLS (36), which combined with our findings, suggests that muscle atrophy plateaus following approximately two weeks of unloading.

Ubiquitin-proteasome-dependent proteolysis is a critical mechanism mediating protein degradation during muscle wasting (37). One of the initial steps in this pathway is the addition of ubiquitin tags via specific ligases. Two E3 ligases specifically found in striated muscle are atrogin-1 and MuRF1, so-called “atrogenes”. These ligases are important mediators of muscle atrophy (38). We found that mRNA levels of atrogin-1 and MuRF1 in mice unloaded for 7 days were 50-100% greater than normally loaded controls. mRNA levels returned to baseline by day 14. Studies of hindlimb immobilization from our group have shown that increased atrogene expression occurs early (day 3-5) and returns to baseline by day 7, although proteasome activity itself remains elevated (27,39). Consistent with these findings, atrogene expression in the tibialis anterior and calf complex have been found elevated with as little as one day of HLS in mice (17).

A potential contributor to the changes in gene expression we observed could be the decreased body weight of mice subjected to HLS. Weight loss during HLS was likely the result of early reductions in food intake (17,40) and fluid loss from diuresis (41). Supporting this, we detected a 13% decrease in fluid mass with HLS. Greater loss of body heat may have also contributed to weight loss via reduction of fat mass, which was also decreased throughout the study. We housed animals at the upper end of the temperature range allowed by the NIH (18−26°C) (42), although this is still below the thermoneutral zone for rodents (26−34°C) (43). Below this range, mice require increased metabolic activity to maintain core temperature. Cachexia has been shown to result in increased expression of the genes encoding atrogin-1 and MuRF1 (44). Compared to the present study, other investigations utilizing the HLS model have demonstrated more modest weight loss in mice, on the order of 2−8% within the first week (17,36). However, these studies were conducted in younger, 10 or 11-week-old female mice. Mice of this age are still in a period of rapid growth (45), a factor that tends to blunt the weight loss experienced during HLS. While weight loss is certainly a confounding factor in the use of HLS as a pure model of mechanical unloading, it

is a relevant variable in the context of its use as a model for the effects of spaceflight. Indeed, a 9% decrease in total body mass was documented in mice of this same age and strain when flown for 15 days on the space shuttle (24). Similarly, 7-week-old mice flown for 13 days on the space shuttle had an average body mass 15% lower than ground controls (46). Astronauts lose approximately 2.4±0.4% body mass per 100 days in space (47). Therefore, although we cannot discount the contribution of weight loss when interpreting these results, it is consistent with spaceflight observations.

Decreased protein synthesis is another important contributor to sarcopenia (48). Muscle protein synthesis was decreased 30−35% by day 7 in mice subjected to HLS. Interestingly, muscle protein synthesis began to recover at day 14 and returned to baseline by day 21. The decline in protein synthesis was limited to the gastrocnemius and quadriceps, as protein synthesis measured in the heart was unchanged. Previously, we showed that hindlimb immobilization results in decreased protein synthesis within 3 days, reaching a peak decline of approximately 25−30% by day 5, with no further decrease by day 7 (27). The restoration of protein synthesis and degradation to baseline levels by the study endpoint suggests that a new homeostatic balance was established. Indeed, there was no additional loss of muscle or lean mass after day 14.

Whereas global muscle protein synthesis returned to control levels after 21 days of unloading, the phosphorylation state of S6K1, a surrogate marker of mTOR activation, was decreased throughout the protocol. Furthermore, 4E-BP1 phosphorylation, which is also downstream of mTOR, was significantly decreased only at day 21, a time when global protein synthesis in muscle from unloaded mice had returned to baseline. The reason for this discordant response in phosphorylation of S6K1 and 4E-BP1 is not clear, but highlights the importance of direct determination of protein synthesis.

The response of the skeletal system to HLS was relatively delayed compared to that of muscle, with significant effects of unloading not apparent until day 14 for trabecular bone and day 21 for cortical bone. Many bone parameters were not different between Control and Suspended groups by the study endpoint. This was particularly apparent in the trabecular compartment, where microstructural parameters tended to reach a peak difference at day 14, before converging at day 21. This response pattern was the result of a decline in the trabecular bone of normally loaded mice over time. Mice of this age were selected because of their skeletal maturity and having reached peak bone mass (49). Comprehensive studies of age-related bone loss in C57BL6/J mice corroborate our findings (45,50). These studies found a large and continuous decline in trabecular bone microstructural beginning at 1.5 months of age. BALB/c mice experience a similar decline beginning at 4 months of age (51). The ability to resolve the effects of HLS on trabecular bone is complicated by this natural deterioration. However, one must consider the average age of an astronaut is now 40-50 years, and trabecular bone in individuals of this age is also undergoing a relatively constant decline (52). Thus, the contribution of aging superimposed on unloading is a consideration in modeling spaceflight. Practically, to resolve differences in trabecular bone between Suspended and Control mice it may be worthwhile to select a two-week period of HLS. Conversely, murine aging studies have documented that cortical bone indices slowly increase until approximately 6 months of age, remaining relatively stable thereafter (45,50).

As a result, resolving differences in this compartment may be achieved with a three-week protocol.

While structural parameters are important, bone strength is ultimately most relevant as regards fracture risk. Bone strength, as assessed using a three-point bending protocol, is primarily dependent on the structure of cortical bone. Our findings for the femur largely reflect this association, with significantly lower mechanical properties generally not appearing until day 14 (the time point when cortical bone changes were first observed). Ultimate bending moment and bending rigidity were decreased by day 14, with further decreases by day 21. Interestingly, we saw significantly lower stress and non-significant changes indicating lower ultimate bending energy at day 7, suggesting that changes in mechanical properties may be manifested even without major structural changes. The stress parameter is an assessment of the material properties of the bone. It is likely that defects in mineralization or collagen content manifest prior to loss of actual bone mass.

Despite similar and significant changes in cortical bone structure, we did not detect an effect of unloading on mechanical properties of the tibia. This study represents the first assessment of the effect of unloading on tibia mechanical properties. Although the mouse tibia's large flat side allows it to be reproducibly positioned for three-point bending, it has several notable limitations for bending analysis that likely increased error and variability. For example, the cross sectional geometry is less symmetrical than the femur, leading to less certainty in stress-at-failure predictions. Additionally the cross section is variable longitudinally, making MicroCT and mechanical testing results sensitive to identification of the tibial midspan (53). It is possible that differences in structure and morphology (e.g., diamond-shaped tibia vs. oval-shaped femur cross-section) mean that a similar relative loss of cortical bone does not translate to a similar loss of strength. It is also possible the testing paradigm we utilized is not appropriate to resolve the mechanical properties of the tibia. Positioning the bone in the anterior-posterior direction or utilizing an alternative testing methodology such as torsion testing may also be warranted.

During unloading, changes in muscle preceded those in bone. This in itself suggests that sarcopenia may contribute to subsequent osteopenia. MicroCT is able to resolve changes in bone structure on the order of 10.5 μm, as compared to the relatively less precise measurements of muscle mass and ^{1}H-NMR. Therefore, the “bone lag” observed during HLS is not an artifact owing to lower skeletal assay resolution. Despite the fact that muscle is directly attached to cortical bone, we observed that trabecular bone loss during HLS tended to be greater in magnitude and precede cortical bone loss. This suggests that trabecular bone is more sensitive to unloading and that the direct effect of reduced weight bearing may be relatively more important to trabecular bone than the effect of reduced muscle forces. Conversely, it may be that trabecular bone, owing to its higher turnover and metabolic activity (54,55), is more sensitive to myokines or other catabolic factors released by sarcopenic muscle during unloading (56). It has been documented that HLS results in reduced functional and isolated muscle strength within 1-3 days after unloading (17), which may contribute to the negative impact of unloading on the underlying cortical bone. Indeed, although bone formation is primarily maintained through weight bearing, the force exerted by muscle on its bony attachments also makes a contribution (20). For example, Turner *et*

al. has shown the posterior eminence of the tibia, a site of high muscle stress, is affected little by HLS and spaceflight, while the anterior aspect of the tibia, which experiences less muscle activity, is severely affected (57). The functional relationship between muscle and bone is also highlighted in the changes we observed in normally loaded control mice. There was no change in cortical bone or muscle mass over time in controls, while trabecular bone declined steadily. Taken together, muscle forces appear to be relatively more important for cortical than trabecular bone during aging and disuse, although the role of muscle-derived bone catabolic factors warrants further study.

The interaction of muscle and bone physiology has received increasing attention in recent years (58,59), with mounting evidence suggesting a dominant role for muscle over bone in the homeostatic maintenance of these two tissues (14). For example, muscle size is strongly correlated with bone size and strength in humans (60). Aside from the direct application of force, however, molecular crosstalk between muscle and bone has been suggested as an important mediator of the relative dependence of these two tissues. Experimental evidence suggests that the aforementioned “myokines” may influence the activity of neighboring bone cells (61), such as delaying osteocyte apoptosis (62). Potentially important mediators of bone-muscle crosstalk include prostaglandin E2 (63), interleukin-6 (64), bone morphogenetic proteins (65), and insulin-like growth factor 1 (66). Genetic co-regulation of muscle and bone may also be regulated by pleiotropic factors, with bone osteoporosis and sarcopenia having a common genetic etiology (67). While the mechanical forces exerted by muscle on bone are certainly important, it is clear that more complicated mechanisms also make a contribution and could a potential focus of therapeutic intervention.

In summary, we have demonstrated that sarcopenia precedes osteopenia during unloading. These data suggest that muscle atrophy may contribute to subsequent skeletal deterioration, particularly in the cortical bone compartment. In addition, the natural decline of trabecular bone with age in normally loaded control mice tends to reduce the magnitude of the effect of HLS, with many trabecular microstructural parameters in unloaded mice converging with controls by day 21. Extension of our findings suggests that a therapeutic strategy that targets muscle may also help to preserve bone during unloading. Taken together, this study has refined the appropriate use of the HLS model, while providing new insights into the development of effective countermeasures to the musculoskeletal effects of spaceflight, prolonged bed rest, and disuse.

Acknowledgments

Funding was provided by grant MA02802 from the National Space Biomedical Research Institute as well as R01 AG013087 and R01 GM38032 from the National Institute on Aging. We thank Anne Pruznak, Maithili Navaratnarajah, and Gina Deiter for their technical assistance.

Authors roles: Study design: SAL, CHL, HJD; Study conduct: SAL, CHL, YZ, EMP, LJL; Data collection: SAL, CHL, YZ, EMP, LJL, GSL; Data interpretation: SAL, CHL, EMP, GSL, HJD; Drafting manuscript: SAL, CHL, HJD; Revising manuscript: SAL, CHL, YZ, EMP, LJL, GSL, HJD; Approving final manuscript: SAL, CHL, YZ, EMP, LJL, GSL, HJD. SAL, CHL, and HJD take responsibility for the integrity of the data analysis.

REFERENCES

1. Lee TQ, Shapiro TA, Bell DM. Biomechanical properties of human tibias in long-term spinal cord injury. J Rehabil Res Dev. 1997; 34(3):295–302. [PubMed: 9239622]
2. Spector ER, Smith SM, Sibonga JD. Skeletal effects of long-duration head-down bed rest. Aviat Space Environ Med. 2009; 80(5 Suppl):A23–8. [PubMed: 19476166]
3. Lang T, LeBlanc A, Evans H, Lu Y, Genant H, Yu A. Cortical and trabecular bone mineral loss from the spine and hip in long-duration spaceflight. Journal of bone and mineral research : the official journal of the American Society for Bone and Mineral Research. 2004; 19(6):1006–12.
4. Lang TF, Leblanc AD, Evans HJ, Lu Y. Adaptation of the proximal femur to skeletal reloading after long-duration spaceflight. Journal of bone and mineral research : the official journal of the American Society for Bone and Mineral Research. 2006; 21(8):1224–30.
5. Bikle DD, Halloran BP. The response of bone to unloading. J Bone Miner Metab. 1999; 17(4):233–44. [PubMed: 10575587]
6. Tesch PA, Berg HE, Bring D, Evans HJ, LeBlanc AD. Effects of 17-day spaceflight on knee extensor muscle function and size. European journal of applied physiology. 2005; 93(4):463–8. [PubMed: 15517339]
7. LeBlanc A, Rowe R, Schneider V, Evans H, Hedrick T. Regional muscle loss after short duration spaceflight. Aviation, space, and environmental medicine. 1995; 66(12):1151–4.
8. Fitts RH, Riley DR, Widrick JJ. Functional and structural adaptations of skeletal muscle to microgravity. The Journal of experimental biology. 2001; 204(Pt 18):3201–8. [PubMed: 11581335]
9. Convertino VA. Physiological adaptations to weightlessness: effects on exercise and work performance. Exercise and sport sciences reviews. 1990; 18:119–66. [PubMed: 2192891]
10. Buehring B, Belavy DL, Michaelis I, Gast U, Felsenberg D, Rittweger J. Changes in lower extremity muscle function after 56 days of bed rest. Journal of applied physiology. 2011; 111(1): 87–94. [PubMed: 21527664]
11. Scott JM, Warburton DE, Williams D, Whelan S, Krassioukov A. Challenges, concerns and common problems: physiological consequences of spinal cord injury and microgravity. Spinal Cord. 2011; 49(1):4–16. [PubMed: 20498665]
12. Orwoll ES, Adler RA, Amin S, Binkley N, Lewiecki EM, Petak SM, Shapses SA, Sinaki M, Watts NB, Sibonga JD. Skeletal health in long-duration astronauts: Nature, assessment and management recommendations from the NASA bone summit. J Bone Miner Res. 2013
13. LeBlanc A, Schneider V. Countermeasures against space flight related bone loss. Acta Astronaut. 1992; 27:89–92. [PubMed: 11537604]
14. Digirolamo DJ, Kiel DP, Esser KA. Bone and skeletal muscle: neighbors with close ties. J Bone Miner Res. 2013
15. Morey-Holton ER, Globus RK. Hindlimb unloading rodent model: technical aspects. Journal of applied physiology. 2002; 92(4):1367–77. [PubMed: 11895999]
16. Colleran PN, Wilkerson MK, Bloomfield SA, Suva LJ, Turner RT, Delp MD. Alterations in skeletal perfusion with simulated microgravity: a possible mechanism for bone remodeling. J Appl Physiol. 2000; 89(3):1046–54. [PubMed: 10956349]
17. Hanson A, Harrison B, Young M, Stodieck L, Ferguson V. Longitudinal Characterization of Functional, Morphologic, and Biochemical Adaptations in Mouse Skeletal Muscle with Hindlimb Suspension. Muscle Nerve Accepted Article. 2013 (Epub: 14 Dec 2012).
18. Lloyd SA, Lewis GS, Zhang Y, Paul EM, Donahue HJ. Connexin 43 deficiency attenuates loss of trabecular bone and prevents suppression of cortical bone formation during unloading. J Bone Miner Res. 2012
19. Warner SE, Sanford DA, Becker BA, Bain SD, Srinivasan S, Gross TS. Botox induced muscle paralysis rapidly degrades bone. Bone. 2006; 38(2):257–64. [PubMed: 16185943]
20. Gross TS, Poliachik SL, Prasad J, Bain SD. The effect of muscle dysfunction on bone mass and morphology. J Musculoskelet Neuronal Interact. 2010; 10(1):25–34. [PubMed: 20190377]

21. Sharir A, Stern T, Rot C, Shahar R, Zelzer E. Muscle force regulates bone shaping for optimal load-bearing capacity during embryogenesis. Development. 2011; 138(15):3247–59. [PubMed: 21750035]
22. Lang TF. The bone-muscle relationship in men and women. J Osteoporos. 2011; 2011:702735. [PubMed: 22007336]
23. Lloyd SA, Bandstra ER, Willey JS, Riffle SE, Tirado-Lee L, Nelson GA, Pecaut MJ, Bateman TA. Effect of proton irradiation followed by hindlimb unloading on bone in mature mice: a model of long-duration spaceflight. Bone. 2012; 51(4):756–64. [PubMed: 22789684]
24. Blaber E, Dvorochkin C, Lee C, Alwood J, Yousuf R, Pianetta P, Globus R, Burns B, Almeida E. Microgravity Induces Pelvic Bone Loss through Osteoclastic Activity, Osteocytic Osteolysis, and Osteoblastic Cell Cycle Inhibition by CDKN1a/p21. PLoS One. 2013; 8(4):1–15.
25. Hargens AR, Steskal J, Johansson C, Tipton CM. Tissue fluid shift, forelimb loading, and tail tension in tail suspended rats. Physiologist. 1984; 27:S37–S38.
26. Vary TC, Lang CH. Assessing effects of alcohol consumption on protein synthesis in striated muscles. Methods Mol Biol. 2008; 447:343–55. [PubMed: 18369928]
27. Lang SM, Kazi AA, Hong-Brown L, Lang CH. Delayed recovery of skeletal muscle mass following hindlimb immobilization in mTOR heterozygous mice. PLoS One. 2012; 7(6):e38910. [PubMed: 22745686]
28. Livak KJ, Schmittgen TD. Analysis of relative gene expression data using real-time quantitative PCR and the 2(-Delta Delta C(T)) Method. Methods. 2001; 25(4):402–8. [PubMed: 11846609]
29. Bouxsein ML, Boyd SK, Christiansen BA, Guldberg RE, Jepsen KJ, Muller R. Guidelines for assessment of bone microstructure in rodents using micro-computed tomography. J Bone Miner Res. 2010; 25(7):1468–86. [PubMed: 20533309]
30. Lang DH, Sharkey NA, Lionikas A, Mack HA, Larsson L, Vogler GP, Vandenbergh DJ, Blizard DA, Stout JT, Stitt JP, McClearn GE. Adjusting data to body size: a comparison of methods as applied to quantitative trait loci analysis of musculoskeletal phenotypes. J Bone Miner Res. 2005; 20(5):748–57. [PubMed: 15824847]
31. Brodt MD, Ellis CB, Silva MJ. Growing C57Bl/6 mice increase whole bone mechanical properties by increasing geometric and material properties. J Bone Miner Res. 1999; 14(12):2159–66. [PubMed: 10620076]
32. Silva MJ, Brodt MD, Lynch MA, McKenzie JA, Tanouye KM, Nyman JS, Wang X. Type 1 diabetes in young rats leads to progressive trabecular bone loss, cessation of cortical bone growth, and diminished whole bone strength and fatigue life. J Bone Miner Res. 2009; 24(9):1618–27. [PubMed: 19338453]
33. Frost RA, Lang CH. mTor signaling in skeletal muscle during sepsis and inflammation: where does it all go wrong? Physiology (Bethesda). 2011; 26(2):83–96. [PubMed: 21487027]
34. LeBlanc A, Lin C, Shackelford L, Sinitsyn V, Evans H, Belichenko O, Schenkman B, Kozlovskaya I, Oganov V, Bakulin A, Hedrick T, Feeback D. Muscle volume, MRI relaxation times (T2), and body composition after spaceflight. J Appl Physiol. 2000; 89(6):2158–64. [PubMed: 11090562]
35. Hanson AM, Ferguson VL, Simske SJ, Cannon CM, Stodieck l S. Comparison of tail-suspension and sciatic nerve crush on the musculoskeletal system in young-adult mice. Biomed Sci Instrum. 2005; 41:92–6. [PubMed: 15850088]
36. Ellman R, Spatz J, Cloutier A, Palme R, Christiansen BA, Bouxsein ML. Partial reductions in mechanical loading yield proportional changes in bone density, bone architecture, and muscle mass. J Bone Miner Res. 2013; 28(4):875–85. [PubMed: 23165526]
37. Attaix D, Ventadour S, Codran A, Bechet D, Taillandier D, Combaret L. The ubiquitin-proteasome system and skeletal muscle wasting. Essays Biochem. 2005; 41:173–86. [PubMed: 16250905]
38. Sandri M, Sandri C, Gilbert A, Skurk C, Calabria E, Picard A, Walsh K, Schiaffino S, Lecker SH, Goldberg AL. Foxo transcription factors induce the atrophy-related ubiquitin ligase atrogin-1 and cause skeletal muscle atrophy. Cell. 2004; 117(3):399–412. [PubMed: 15109499]
39. Krawiec BJ, Frost RA, Vary TC, Jefferson LS, Lang CH. Hindlimb casting decreases muscle mass in part by proteasome-dependent proteolysis but independent of protein synthesis. Am J Physiol Endocrinol Metab. 2005; 289(6):E969–80. [PubMed: 16046454]

40. Simske SJ, Broz JJ, Fleet ML, Schmeister TA, Gayles EC, Luttges MW. Contribution of dietary and loading changes to the effects of suspension on mouse femora. J Exp Zool. 1994; 269(3):277–85. [PubMed: 8014618]
41. Deavers DR, Musacchia XJ, Meininger GA. Model for antiorthostatic hypokinesia: head-down tilt effects on water and salt excretion. J Appl Physiol. 1980; 49(4):576–82. [PubMed: 7440274]
42. Morey-Holton ER, Globus RK. Hindlimb unloading rodent model: technical aspects. J Appl Physiol. 2002; 92(4):1367–77. [PubMed: 11895999]
43. C. G. Temperature Regulation in Laboratory Rodents. Cambridge Univ. Press; Cambridge, UK.: 1993.
44. White JP, Baynes JW, Welle SL, Kostek MC, Matesic LE, Sato S, Carson JA. The regulation of skeletal muscle protein turnover during the progression of cancer cachexia in the Apc(Min/+) mouse. PLoS One. 2011; 6(9):e24650. [PubMed: 21949739]
45. Halloran BP, Ferguson VL, Simske SJ, Burghardt A, Venton LL, Majumdar S. Changes in bone structure and mass with advancing age in the male C57BL/6J mouse. J Bone Miner Res. 2002; 17(6):1044–50. [PubMed: 12054159]
46. Baqai FP, Gridley DS, Slater JM, Luo-Owen X, Stodieck LS, Ferguson V, Chapes SK, Pecaut MJ. Effects of spaceflight on innate immune function and antioxidant gene expression. J Appl Physiol. 2009; 106(6):1935–42. [PubMed: 19342437]
47. Matsumoto A, Storch KJ, Stolfi A, Mohler SR, Frey MA, Stein TP. Weight loss in humans in space. Aviat Space Environ Med. 2011; 82(6):615–21. [PubMed: 21702312]
48. Eley HL, Tisdale MJ. Skeletal muscle atrophy, a link between depression of protein synthesis and increase in degradation. J Biol Chem. 2007; 282(10):7087–97. [PubMed: 17213191]
49. Beamer WG, Donahue LR, Rosen CJ, Baylink DJ. Genetic variability in adult bone density among inbred strains of mice. Bone. 1996; 18(5):397–403. [PubMed: 8739896]
50. Glatt V, Canalis E, Stadmeyer L, Bouxsein ML. Age-related changes in trabecular architecture differ in female and male C57BL/6J mice. J Bone Miner Res. 2007; 22(8):1197–207. [PubMed: 17488199]
51. Willinghamm MD, Brodt MD, Lee KL, Stephens AL, Ye J, Silva MJ. Age-related changes in bone structure and strength in female and male BALB/c mice. Calcif Tissue Int. 2010; 86(6):470–83. [PubMed: 20405109]
52. Ding M, Hvid I. Quantification of age-related changes in the structure model type and trabecular thickness of human tibial cancellous bone. Bone. 2000; 26(3):291–5. [PubMed: 10710004]
53. Schriefer JL, Warden SJ, Saxon LK, Robling AG, Turner CH. Cellular accommodation and the response of bone to mechanical loading. J Biomech. 2005; 38(9):1838–45. [PubMed: 16023471]
54. Almeida M, Han L, Martin-Millan M, Plotkin LI, Stewart SA, Roberson PK, Kousteni S, O'Brien CA, Bellido T, Parfitt AM, Weinstein RS, Jilka RL, Manolagas SC. Skeletal involution by age-associated oxidative stress and its acceleration by loss of sex steroids. J Biol Chem. 2007; 282(37): 27285–97. [PubMed: 17623659]
55. Goodyear SR, Gibson IR, Skakle JM, Wells RP, Aspden RM. A comparison of cortical and trabecular bone from C57 Black 6 mice using Raman spectroscopy. Bone. 2009; 44(5):899–907. [PubMed: 19284975]
56. Hamrick MW. A role for myokines in muscle-bone interactions. Exerc Sport Sci Rev. 2011; 39(1): 43–7. [PubMed: 21088601]
57. Turner RT, Wakley GK, Szukalski BW. Effects of gravitational and muscular loading on bone formation in growing rats. Physiologist. 1985; 28(6 Suppl):S67–8. [PubMed: 3834489]
58. Bonewald LF, Kiel DP, Clemens TL, Esser K, Orwoll ES, O'Keefe RJ, Fielding RA. Forum on bone and skeletal muscle interactions: Summary of the proceedings of an ASBMR workshop. J Bone Miner Res. 2013; 28(9):1857–65. [PubMed: 23671010]
59. Brotto M. Lessons from the FNIH-NIA-FDA sarcopenia consensus summit. IBMS Bonekey. 2012; 9
60. Edwards M, Gregson C, Patel H, Jameson K, Harvey N, Sayer AA, Dennison E, Cooper C. Muscle size, strength and physical performance and their associations with bone structure in the Hertfordshire Cohort Study. J Bone Miner Res. 2013

61. Pedersen BK, Febbraio MA. Muscles, exercise and obesity: skeletal muscle as a secretory organ. Nat Rev Endocrinol. 2012; 8(8):457–65. [PubMed: 22473333]

62. Jahn K, Lara-Castillo N, Brotto L, Mo CL, Johnson ML, Brotto M, Bonewald LF. Skeletal muscle secreted factors prevent glucocorticoid-induced osteocyte apoptosis through activation of beta-catenin. Eur Cell Mater. 2012; 24:197–209. discussion 209-10. [PubMed: 22972510]

63. Mo C, Romero-Suarez S, Bonewald L, Johnson M, Brotto M. Prostaglandin E2: from clinical applications to its potential role in bone-muscle crosstalk and myogenic differentiation. Recent Pat Biotechnol. 2012; 6(3):223–9. [PubMed: 23092433]

64. Rufo A, Del Fattore A, Capulli M, Carvello F, De Pasquale L, Ferrari S, Pierroz D, Morandi L, De Simone M, Rucci N, Bertini E, Bianchi ML, De Benedetti F, Teti A. Mechanisms inducing low bone density in Duchenne muscular dystrophy in mice and humans. J Bone Miner Res. 2011; 26(8):1891–903. [PubMed: 21509823]

65. Ruschke K, Hiepen C, Becker J, Knaus P. BMPs are mediators in tissue crosstalk of the regenerating musculoskeletal system. Cell Tissue Res. 2012; 347(3):521–44. [PubMed: 22327483]

66. Tahimic CG, Wang Y, Bikle DD. Anabolic effects of IGF-1 signaling on the skeleton. Front Endocrinol (Lausanne). 2013; 4:6. [PubMed: 23382729]

67. Karasik D, Kiel DP. Evidence for pleiotropic factors in genetics of the musculoskeletal system. Bone. 2010; 46(5):1226–37. [PubMed: 20149904]

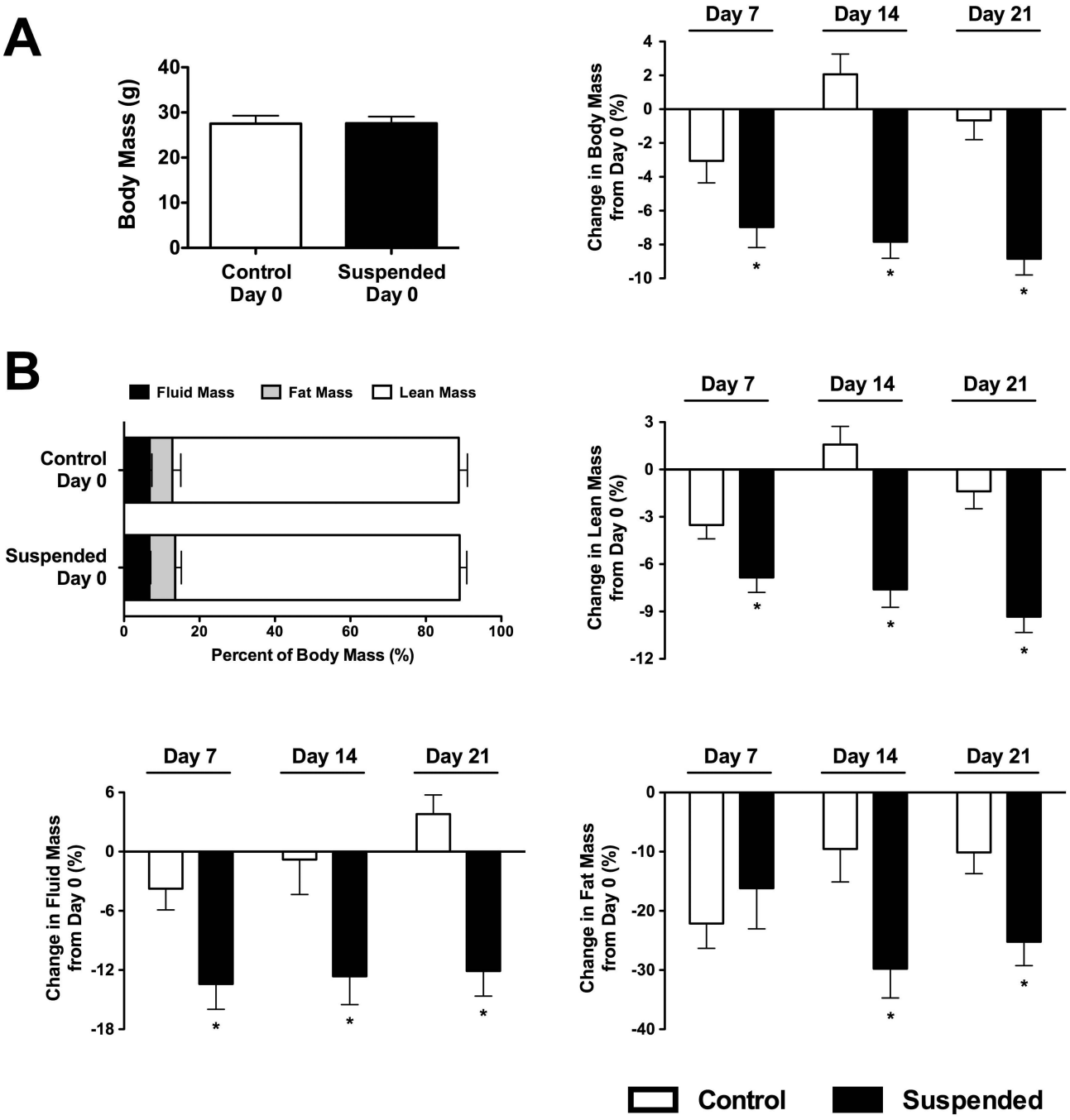

Figure 1.

Body habitus of mice subjected to normal loading (Control) or mechanical unloading via hindlimb suspension (Suspended). (A) (Left) Baseline (Day 0) total body mass of mice assigned to either Control (n=64) or Suspension (n=36). (Right) Percent change in total body mass from day 0 (n=12-16/group). (B) Baseline body composition of mice assigned to either Control (n=64) or Suspension (n=36). Percent change in fluid mass, fat mass, and lean mass from day 0 (n=12-16/group). Data shown as Mean ± SEM. * indicates a significant difference from time-matched Control value ($p<0.05$).

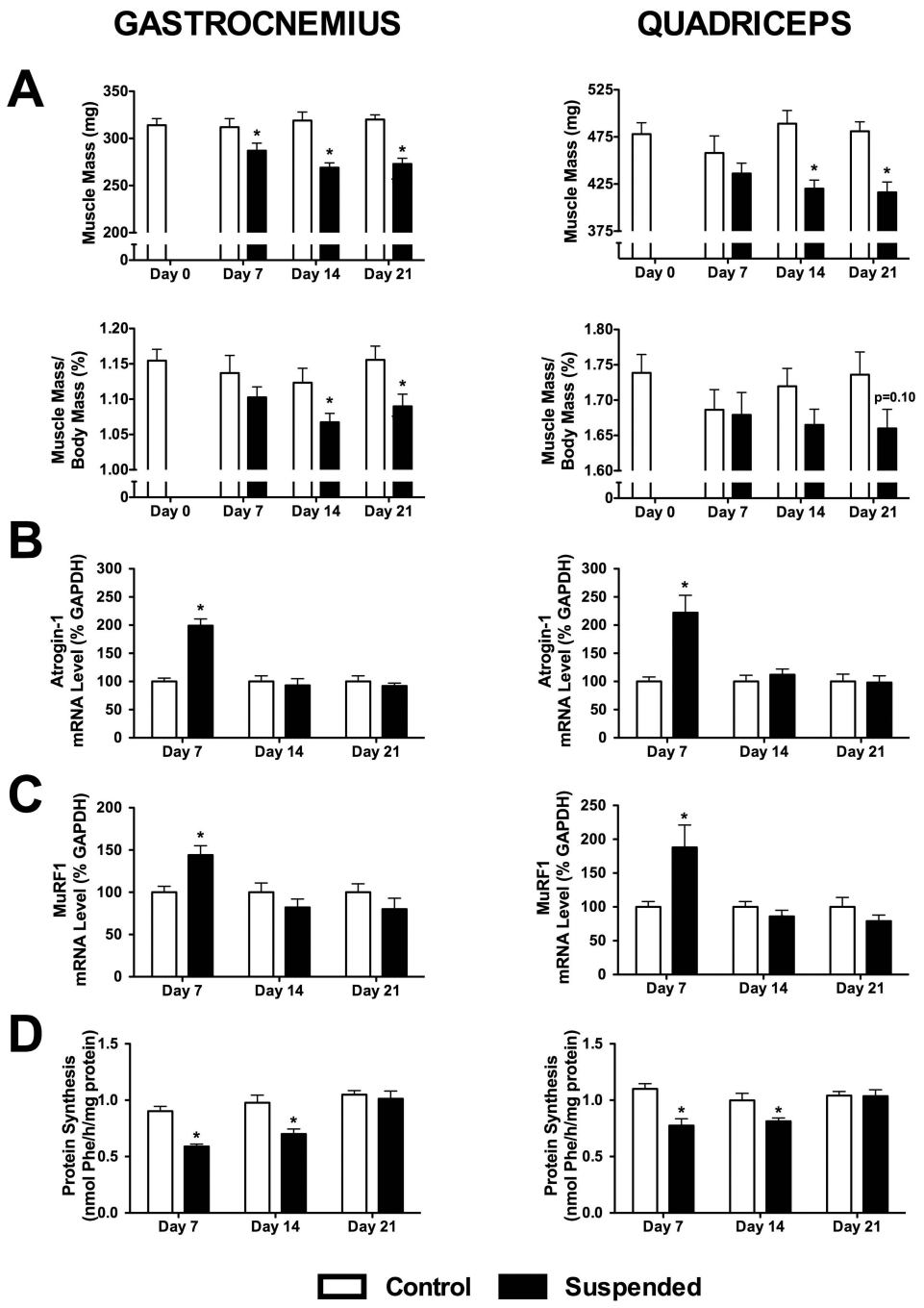

Figure 2.

Muscle properties obtained from mice subjected to normal loading (Control) or mechanical unloading via hindlimb suspension (Suspended). (A) Total muscle mass and muscle mass normalized to body mass, (B) mRNA levels of the gene encoding atrogin-1, (C) mRNA levels of the gene encoding MuRF1, and (D) protein synthesis rates were determined for both the gastrocnemius (left) and quadriceps (right). (n=12-16/group). Data shown as Mean ± SEM. * indicates a significant difference of Suspended from time-matched Control value ($p<0.05$).

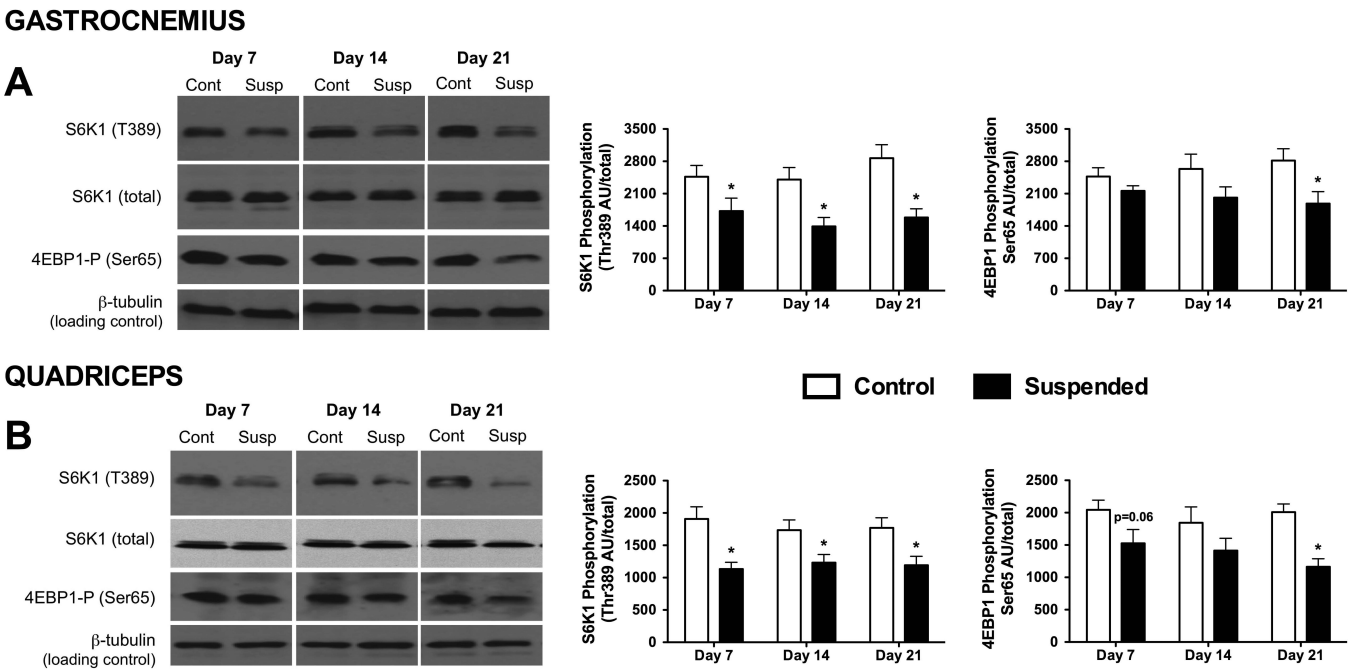

Figure 3.

Alterations in S6K1 and 4E-BP1 phosphorylation of (A) gastrocnemius and (B) quadriceps muscle obtained from mice subjected to normal loading (Control; Cont) or mechanical unloading via hindlimb suspension (Suspended; Susp). There was no significant difference in the total amount of total S6K1and 4E-BP1 between Control and Suspended muscle at any time point (data not shown). (Left) Representative Western blots of phosphorylated and total proteins of interest. Western blots for Control and Suspended muscle from the same time point were run on the same gel. (Right) Densitometric quantitation of all Western blot data. (n=9/group). Data shown as Mean ± SEM. * indicates a significant difference of Suspended from time-matched Control value ($p<0.05$).

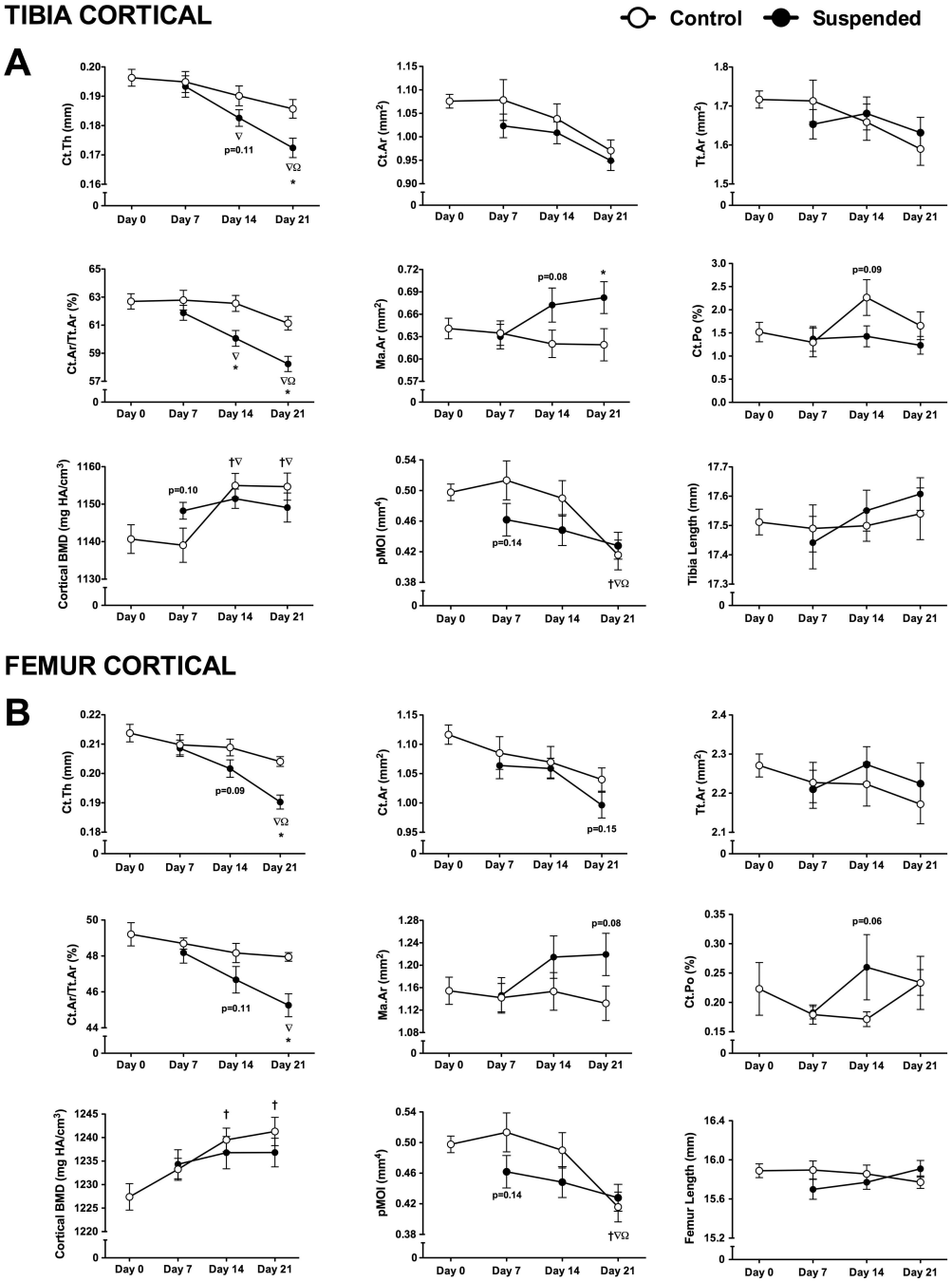

Figure 4.

Cortical microstructural parameters obtained via microcomputed tomography scans of tibias and femurs obtained from mice subjected to normal loading conditions (Control) or mechanical unloading via hindlimb suspension (Suspended). Measured parameters at the tibia midshaft (A) included cortical thickness (Ct.Th), cortical area (Ct.Ar), total area (Tt.Ar), cortical area fraction (Ct.Ar/Tt.Ar), marrow area (Ma.Ar), cortical porosity (Ct.Po), cortical bone mineral density (BMD), polar moment of inertia (pMOI). Length of the tibia was also measured. These parameters were also determined for cortical bone at the femur

midshaft (B). (n=12-16/group). Data shown as Mean ± SEM. Significant difference between two time points within a loading condition (Control or Suspended) is indicated as: † $p<0.05$ vs. Day 0, ∇$p<0.05$ vs. Day 7, Ω $p<0.05$ vs. Day 14, while * indicates a significant difference of Suspended from time-matched Control value ($p<0.05$).

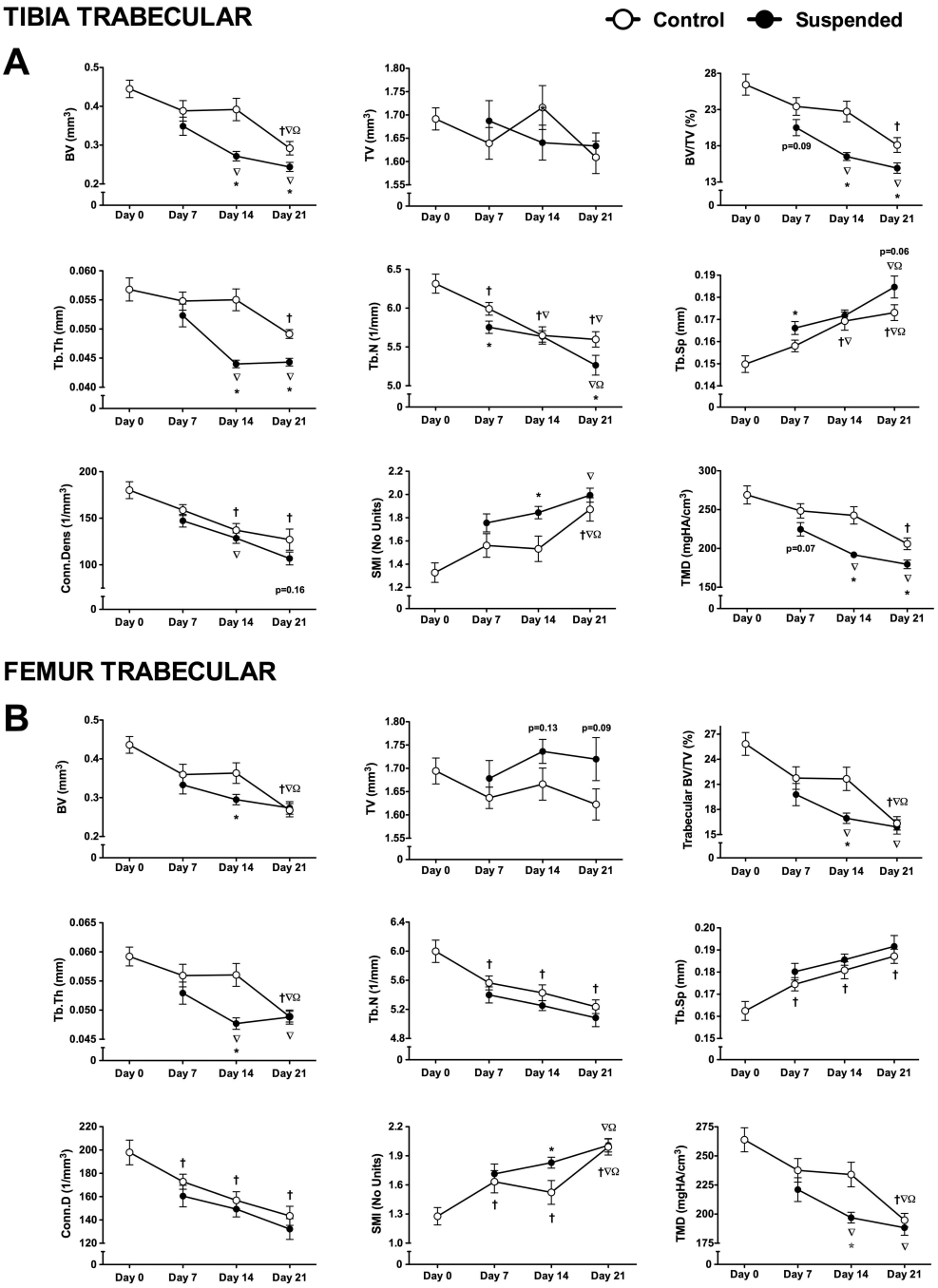

Figure 5.

Trabecular microstructural parameters obtained via microcomputed tomography scans of tibias and femurs obtained from mice subjected to normal loading conditions (Control) or mechanical unloading via hindlimb suspension (Suspended). Measured parameters at the proximal tibia (A) included bone volume (BV), total volume (TV), bone volume fraction (BV/TV), trabecular thickness (Tb.Th), trabecular number (Tb.N), trabecular separation (Tb.Sp), connectivity density (Conn.D), structure model index (SMI), and tissue mineral density (TMD). These parameters were also determined for trabecular bone at the distal

femur (B). (n=12-16/group). Data shown as Mean ± SEM. Significant difference between two time points within a loading condition (Control or Suspended) is indicated as: † $p<0.05$ vs. Day 0, ∇$p<0.05$ vs. Day 7, Ω $p<0.05$ vs. Day 14, while * indicates a significant difference of Suspended from time-matched Control value ($p<0.05$).

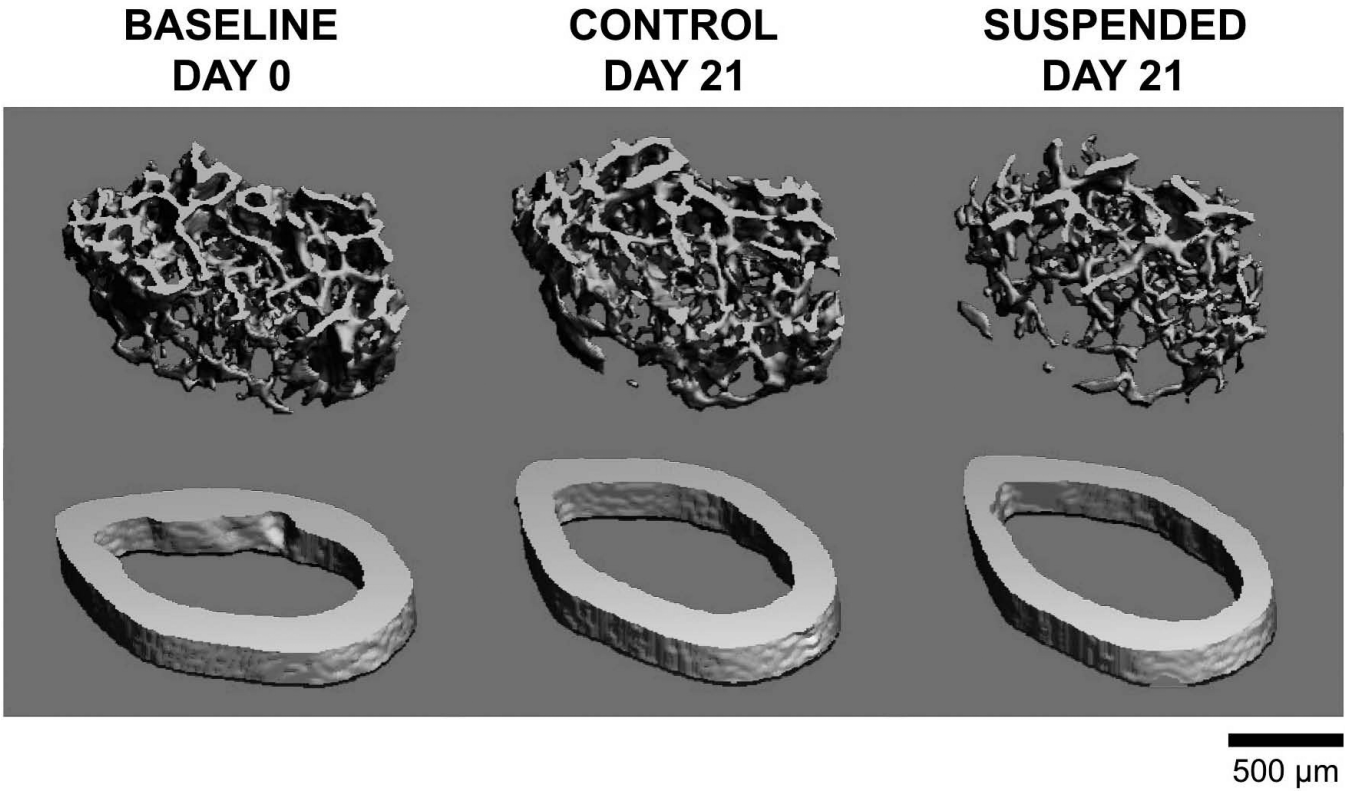

Figure 6.

Representative images of trabecular (top) and cortical (bottom) microstructure from mice subjected to normal loading conditions (Control) or mechanical unloading via hindlimb suspension (Suspended). Representative 3D MicroCT reconstructions were selected based on mean trabecular bone volume fraction or cortical thickness. Trabecular images represent 72 slices (756 μm) of the distal femur, immediately proximal to the epiphyseal plate. Cortical images represent 22 slices (231 μm) of the femur midshaft.

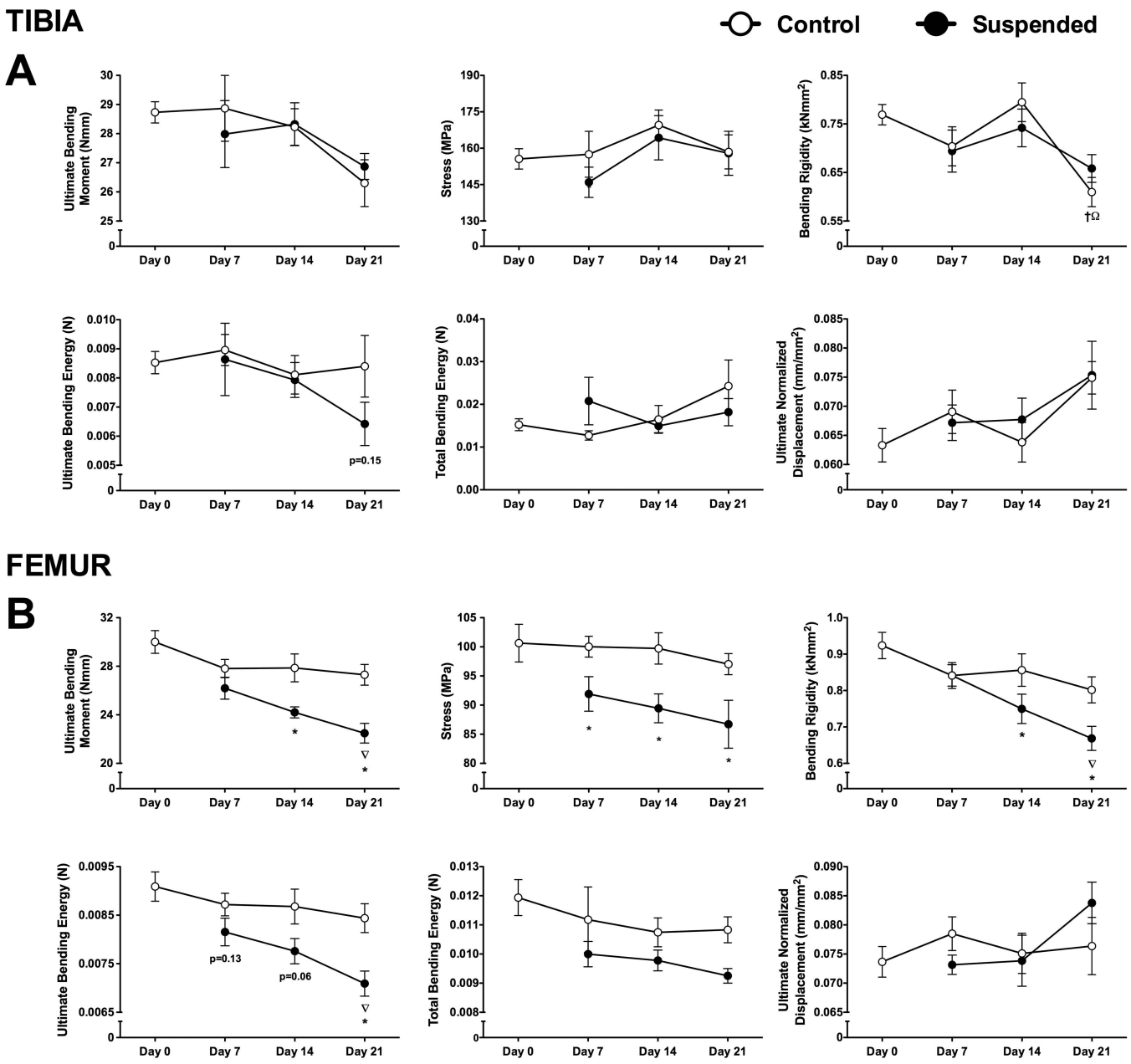

Figure 7.

Bone mechanical properties from mice subjected to normal loading conditions (Control) or mechanical unloading via hindlimb suspension (Suspended). Measured parameters of the tibia (A) included ultimate bending moment, stress, bending rigidity, ultimate bending energy, total bending energy, and ultimate normalized displacement (at maximum force). These parameters were also determined for the femur (B). (n=12-16/group). Data shown as Mean ± SEM. Significant difference between two time points within a loading condition (Control or Suspended) is indicated as: † $p<0.05$ vs. Day 0, ∇$p<0.05$ vs. Day 7, Ω $p<0.05$ vs. Day 14, while * indicates a significant difference of Suspended from time-matched Control value ($p<0.05$).

Table 1

Summary of experimental groups and animal numbers.

Day of Study	Loading Condition	n
Day 0	Control	16
Day 7	Control	16
	Suspended	12
Day 14	Control	16
	Suspended	12
Day 21	Control	16
	Suspended	12